A CORONAL MAGNETIC FIELD MODEL WITH HORIZONTAL VOLUME AND SHEET CURRENTS

XUEPU ZHAO and J. TODD HOEKSEMA

Center for Space Science and Astrophysics, Stanford University, Stanford, CA 94305, U.S.A.

Abstract. When globally mapping the observed photospheric magnetic field into the corona, the interaction of the solar wind and magnetic field has been treated either by imposing source surface boundary conditions that tacitly require volume currents outside the source surface (Schatten, Wilcox, and Ness, 1969) or by limiting the interaction to thin current sheets between oppositely directed field regions (Wolfson, 1985). Yet observations and numerical MHD calculations suggest the presence of non-force-free volume currents throughout the corona as well as thin current sheets in the neighborhoods of the interfaces between closed and open field lines or between oppositely directed open field lines surrounding coronal helmet-streamer structures. This work presents a model including both horizontal volume currents and streamer sheet currents. The present model builds on the magnetostatic equilibria developed by Bogdan and Low (1986) and the current-sheet modeling technique developed by Schatten (1971). The calculation uses synoptic charts of the line-of-sight component of the photospheric magnetic field measured at the Wilcox Solar Observatory. Comparison of an MHD model with the calculated model results for the case of a dipole field and comparison of eclipse observations with calculations for CR 1647 (near solar minimum) show that this horizontal current–current-sheet model reproduces polar plumes and axes of corona streamers better than the source-surface model and reproduces coronal helmet structures better than the current-sheet model.

1. Introduction

In globally mapping the observed photospheric magnetic field into the corona, three approaches have been developed and tested so far. The first is the potential field–source-surface (PFSS) model (Schatten, Wilcox, and Ness, 1969; Altschuler and Newkirk, 1969). In this approach, the effect of the solar wind on the coronal magnetic field is modeled by assuming that above a 'source-surface' at some height, the magnetic field becomes strictly radial. This model is the most widely used and has been successful in comparing the calculated magnetic field with density structures in the corona (Altschuler and Newkirk, 1969) and with the interplanetary magnetic field (Schatten, Wilcox, and Ness, 1969), in calculating the position of coronal holes (Levine *et al.*, 1977) and the heliospheric current sheet (Hoeksema, Wilcox, and Scherrer, 1982), and in predicting the solar wind speed (Levine *et al.*, 1977; Wang and Sheeley, 1990). However, the magnetic field lines predicted using the PFSS model at middle and high latitudes (see panel 2 of Figure 1) do not closely match the observations of polar plumes or the axes of coronal streamers, which are supposed to track the paths of magnetic field lines (see panel 1 of Figure 1).

The second approach is the potential field–current-sheet (PFCS) model (Schatten, 1971). This model extends a pure potential field beyond a given radius in a way that requires the presence of current sheets between the oppositely directed open field lines. As shown in the bottom panel of Figure 1, the predicted field lines

Panel 1

Panel 2   a = 0. 0
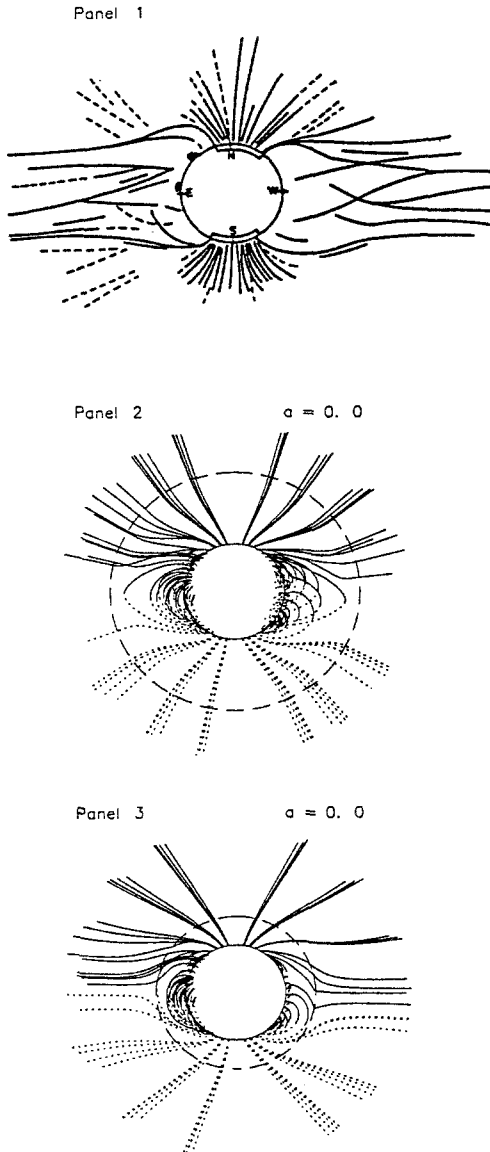

Panel 3   a = 0. 0

Fig. 1. Comparison of the original drawing of the solar total eclipse observed on 23 October, 1976 (*top*) (Loucif and Craag, 1988) with the magnetic field structures predicted using the source-surface model (*middle*), and the current-sheet model (*bottom*). The near-limb field lines in the model should outline density structures observed during the eclipse.

using this model agree with the observations best for the polar plumes and the axes of streamers. The predicted closed regions at low latitudes are obviously smaller than the observed coronal helmets (panel 1).

The third approach, taken by Zhao and Hoeksema (1992), may be called the

horizontal current–source-surface (HCSS) model. It builds on the magnetostatic equilibria developed by Bogdan and Low (1986) and the 'source surface' technique. The magnetic configuration predicted by this model is basically the same as the PFSS model though it can calculate the plasma properties in the corona as well.

In deciding how to further improve the existing models, it may be instructive to compare these models with a full MHD model of plasma–magnetic field interactions. In modeling the solar wind–magnetic field interaction, the classic work of Pneuman and Kopp (1971) solved the steady-state MHD problem iteratively to obtain a self-consistent solution in which magnetic force, gas pressure, gravity, and solar wind acceleration everywhere satisfy the momentum equation. The Pneuman and Kopp solution results in horizontal volume currents throughout the corona, as well as current sheets in the helmet interface separating closed and open field lines and in the streamer interface separating oppositely directed open field lines. These electric currents open up the field lines at high latitudes and expand the field lines at low latitudes, distending the magnetic dipole field into a non-potential dipole-like field (see Figure 8 of Pneuman and Kopp's paper). Because the MHD model is a self-consistent solution of both the solar wind and magnetic field, the model remains a paradigm against which subsequent work has been compared.

Figure 1 of Newkirk (1972) showed that between the solar surface and source surface the PFSS model matches the non-potential field calculated from the MHD solution very well, especially in the closed field regions at low latitudes. Introducing a 'source surface' amounts to assuming that all coronal currents are outside the source-surface, beyond which the magnetic field is assumed to be radial and hence the current is toroidal, without a radial component. Thus the source-surface technique attempts to substitute the volume and sheet currents flowing in the corona with volume currents flowing in the outer corona to model the effect of the solar wind outflow on the magnetic field.

The relatively poor agreement for open field lines at higher altitude indicates that the source-surface technique improperly models the effect of sheet currents on the magnetic field lines. Specifically it does not model the radial distension of the field lines at different heliocentric distances that increases with increasing latitude. On the other hand, Figure 6 of Schatten (1971) showed that the prediction of the PFCS model agrees with the MHD solution best for open field lines at higher altitudes. However, significant disagreement occurs at lower altitude, especially for closed field lines, indicating the necessity of including horizontal volume currents to expand the closed field.

Our goal is to develop a flexible, physically more realistic model that uses photospheric magnetic field observations (such as those that will be provided by the Solar Oscillations Investigator–Michelson Doppler Imager on SOHO) to produce a somewhat more quantitative model of the coronal magnetic field. Because the magnetic field plays a critical role in determining the structure and dynamics of the corona, the results of such a coronal magnetic field model will be essential for interpreting the results of many of the experiments on SOHO and Ulysses.

In this study, we take a preliminary step in this direction. We present here a new model that incorporates effects of both horizontal volume currents and external sheet currents referred to as the 'horizontal current–current-sheet' or HCSS model. The predictions of the HCSS model agree with observations better than either the PFSS model or the PFCS model.

2. Model

The purpose of coronal–heliospheric modeling is to determine what happens in the corona and heliosphere from observed conditions on the solar surface and a deterministic set of physical laws. Specification of the boundary conditions on the solar surface implies that the physical quantities specified there are overwhelmingly determined by the physical processes operating below the solar surface. To first approximation, the magnetic field and plasma properties can be assumed to vanish on an outer surface of infinite radius. As clearly indicated by helmet-streamer structures observed in solar eclipses (see Figure 1), the greatest effect of currents in the corona is their alteration of the magnetic topology as shown by the fact that many magnetic field lines are distended to form open configurations. Full MHD solutions (Pneuman and Kopp, 1971; Steinolfson, Suess, and Wu, 1982) have shown that a streamer interface starts near the cusp-type neutral point just overlying a closed region and the coronal expansion across the cusp point transforms from sub-Alfvénic to super-Alfvénic.

We assume that the coronal currents consist of horizontal volume currents flowing everywhere in the corona and sheet currents flowing within streamer interfaces. In addition, all helmet-streamer cusp points are constrained to have identical heliocentric distance, R_{cp}. Based on the current sheet modeling technique developed by Schatten (1971), we divide the corona into two regions separated by a spherical surface located near the cusp points of coronal helmet streamers, $r = R_{cp}$. To distinguish it from the 'source surface' adopted in the PFSS and PFCS models, we call it the 'cusp surface'.

The HCCS model builds on a magnetostatic atmosphere instead of the potential field. When electric currents flow perpendicular to the solar gravity everywhere, a set of solutions to the magnetostatic equation

$$\frac{1}{4\pi}(\nabla \times \mathbf{B}) \times \mathbf{B} - \nabla p - \rho \frac{GM}{r^2}\hat{r} = 0 \tag{1}$$

has been found (Low, 1985; Bogdan and Low, 1986) for the magnetic field, $\mathbf{B}$, plasma pressure, p, and plasma density, ρ, that depend on an unknown function $\Phi(r, \theta, \phi)$ as

$$\mathbf{B} = -\eta(r)\frac{\partial \Phi}{\partial r}\hat{r} - \frac{1}{r}\frac{\partial \Phi}{\partial \theta}\hat{\theta} - \frac{1}{r\sin\theta}\frac{\partial \Phi}{\partial \phi}\hat{\phi}, \tag{2}$$

$$p = p_0(r) + \frac{1}{8\pi}\eta(r)[1 - \eta(r)]\left(\frac{\partial\Phi}{\partial r}\right)^2 , \tag{3}$$

$$\rho = \rho_0(r) + \frac{1}{GM}\left\{\frac{\eta(r) - 1}{8\pi}\frac{\partial}{\partial r}\left(\frac{\partial\Phi}{\partial\theta}\right)^2 + \right.$$

$$+\frac{1}{8\pi}\frac{\eta(r) - 1}{\sin^2\theta}\frac{\partial}{\partial r}\left(\frac{\partial\Phi}{\partial\phi}\right)^2 +$$

$$\left.+\frac{r^2}{8\pi}\frac{\partial}{\partial r}\left[\eta(r)\left[\eta(r) - 1\right]\left(\frac{\partial\Phi}{\partial r}\right)^2\right]\right\} , \tag{4}$$

where

$$\eta(r) = \left(1 + \frac{a}{r}\right)^2 . \tag{5}$$

The parameter a in Equation (5) is a free parameter related to a scalelength of the horizontal electric current, and $\rho_0(r)$ is a free function representing a background dnesity with spherical symmetry. The background pressure is related to the background density by $p_0(r) = -\int_r^\infty dl GM\rho_0(l)/l^2$.

We formulate solutions appropriate to each of two regions and require that all three components of the magnetic field be continuous across the cusp surface.

In the inner region between the solar surface and the cusp surface, the unknown function Φ in Equations (2)–(4) can be expressed as

$$\Phi = \sum_{n=1}^{N_\odot}\sum_{m=0}^{n} R_n^\odot(r)P_n^m(\cos\theta)\left(g_{nm}^\odot\cos m\phi + h_{nm}^\odot\sin m\phi\right) , \tag{6}$$

$$R_n^\odot(r) = \frac{R_\odot(1 + a)^n}{(n + 1)(r + a)^{n+1}} , \tag{7}$$

where $N_\odot$ is the maximum principal index, $P_n^m(\cos\theta)$ are the associated Legendre polynomials with Schmidt normalization, and the spherical-harmonic-expansion coefficients of the photospheric magnetic field, $g_{nm}^\odot$ and $h_{nm}^\odot$, can be determined by the observed line-of-sight component of the photospheric field, B_{ls},

$$g_{nm}^\odot = \frac{2n + 1}{IJ}\sum_{i=1}^{I}\sum_{j=1}^{J} B_{ls}(\theta_i, \phi_j)P_n^m(\theta_i)\cos(m\phi_j)/\sin\theta_i , \tag{8}$$

$$h_{nm}^\odot = \frac{2n + 1}{IJ}\sum_{i=1}^{I}\sum_{j=1}^{J} B_{ls}(\theta_i, \phi_j)P_n^m(\theta_i)\sin(m\phi_j)/\sin\theta_i . \tag{9}$$

Here we assume that the photospheric field is radial because there is evidence that the field is radially dominated (Wang and Sheeley, 1992, and references therein). In Equations (8) and (9), I and J are, respectively, the number of latitudinal and longitudinal grid points. We select $I = 30$ and $J = 72$ in the following calculation. By using above expressions we calculate the three components of the magnetic field at the cusp surface, and reverse the direction of the calculated **B** wherever $B_r(R_{cp}, \theta, \phi) < 0$. This reversal procedure is used in the Schatten's technique to obtain the inner boundary condition for solutions in the outer region, i.e., the $(I \times J \times 3) \times 1$ matrix in Equation (12),

$$
\overline{B} =
\begin{bmatrix}
B(\theta_1, \phi_1, 1) \\
B(\theta_1, \phi_2, 1) \\
\vdots \\
B(\theta_1, \phi_J, 1) \\
B(\theta_1, \phi_1, 2) \\
\vdots \\
B(\theta_I, \phi_J, 3)
\end{bmatrix},
$$

where $k = 1$, 2, or 3 in $B(\theta, \phi_i, k)$ refers to the radial, latitudinal, or azimuthal field components at $(R_{cp}, \theta_i, \phi_i)$. Such a boundary condition ensures that the calculated field lines are open everywhere beyond the cusp surface.

In the outer region, we use following expressions to calculate the magnetic field beyond the cusp surface:

$$
\Phi = \sum_{n=0}^{N_c} \sum_{m=0}^{n} R_n^c(r) P_n^m (\cos \theta) \left(g_{nm}^c \cos m\phi + h_{nm}^c \sin m\phi \right),
\tag{10}
$$

$$
R_n^c(r) = \frac{R_\odot R_{cp}^2 (R_{cp} + a)^n}{(n + 1)(r + a)^{n+1}},
\tag{11}
$$

where N_c is the maximum principal index, and the spherical-harmonic-expansion coefficients of the magnetic field (that points outward everywhere on the cusp surface) can be expressed, with all $m = 0$ elements missing from h_{nm}^c, as $(N + 1)^2 \times 1$ matrix:

$$\overline{gh} = \begin{bmatrix} g_{00}^c \\ g_{10}^c \\ \vdots \\ g_{NN}^c \\ h_{11}^c \\ h_{21}^c \\ \vdots \\ h_{NN}^c \end{bmatrix} .$$

The coefficients are obtained by applying a least-squares matching procedure (see Appendix I of Schatten, 1971):

$$\overline{gh} = \overline{AB}^{-1} \cdot \overline{\alpha\beta} \cdot \overline{B} . \tag{12}$$

Here $\overline{\alpha\beta}$ in Equation (12) is a $(N+1)^2 \times (I \cdot J \cdot 3)$ matrix with all $m = 0$ elements missing from $\beta_{n\,m,\,\theta_i,\,\phi_j,\,k}$,

$$\overline{\alpha\beta} = \begin{bmatrix} \alpha_{0,0,\theta_1,\phi_1,1} & \alpha_{0,0,\theta_1,\phi_1,1} & \cdots & \alpha_{0,0,\theta_J,\phi_J,1} & \alpha_{0,0,\theta_1,\phi_1,2} & \cdots & \alpha_{0,0,\theta_I,\phi_J,3} \\ \alpha_{1,0,\theta_1,\phi_1,1} & \alpha_{1,0,\theta_1,\phi_1,1} & \cdots & \alpha_{1,0,\theta_J,\phi_J,1} & \alpha_{1,0,\theta_1,\phi_1,2} & \cdots & \alpha_{1,0,\theta_I,\phi_J,3} \\ \vdots & \vdots & & \vdots & \vdots & & \vdots \\ \alpha_{N,N,\theta_1,\phi_1,1} & \alpha_{N,N,\theta_1,\phi_2,1} & \cdots & \alpha_{N,N,\theta_1,\phi_J,1} & \alpha_{N,N,\theta_1,\phi_1,2} & \cdots & \alpha_{N,N,\theta_I,\phi_J,3} \\ \beta_{1,1,\theta_1,\phi_1,1} & \beta_{1,1,\theta_1,\phi_2,1} & \cdots & \beta_{1,1,\theta_1,\phi_J,1} & \beta_{1,1,\theta_1,\phi_1,2} & \cdots & \beta_{1,1,\theta_I,\phi_J,3} \\ \beta_{2,1,\theta_1,\phi_1,1} & \beta_{2,1,\theta_1,\phi_2,1} & \cdots & \beta_{2,1,\theta_1,\phi_J,1} & \beta_{2,1,\theta_1,\phi_1,2} & \cdots & \beta_{2,1,\theta_I,\phi_J,3} \\ \vdots & \vdots & & \vdots & \vdots & & \vdots \\ \beta_{N,N,\theta_1,\phi_1,1} & \beta_{N,N,\theta_1,\phi_2,1} & \cdots & \beta_{N,N,\theta_1,\phi_J,1} & \beta_{N,N,\theta_1,\phi_1,2} & \cdots & \beta_{N,N,\theta_I,\phi_J,3} \end{bmatrix} ,$$

where

$$\alpha_{n,\,m,\,\theta_i,\,\phi_j,\,1} = \cos(m\phi_j) P_n^m(\theta_i) ,$$

$$\beta_{n,\,m,\,\theta_i,\,\phi_j,\,1} = \sin(m\phi_j) P_n^m(\theta_i) ,$$

$$\alpha_{n,\,m,\,\theta_i,\,\phi_j,\,2} = -K_n \cos(m\phi_j) \frac{\mathrm{d}P_n^m(\theta_i)}{\mathrm{d}\theta} ,$$

$$\beta_{n,\,m,\,\theta_i,\,\phi_j,\,2} = -K_n \sin(m\phi_j) \frac{\mathrm{d}P_n^m(\theta_i)}{\mathrm{d}\theta} ,$$

$$\alpha_{n,\,m,\,\theta_i,\,\phi_j,\,3} = mK_n \sin(m\phi_j) \frac{P_n^m(\theta_i)}{\sin(\theta_i)} ,$$

$$\beta_{n, m, \theta_i, \phi_j, 3} = -mK_n \cos(m\phi_j)\frac{P_n^m(\theta_i)}{\sin(\theta_i)} ,$$

$$K_n = \frac{R_{cp}}{(n + 1)(R_{cp} + a)} .$$

In Equation (12) $\overline{AB}^{-1}$ is the inversion of the symmetric matrix $\overline{AB}$, and $\overline{AB} = \overline{\alpha\beta} \cdot \overline{\alpha\beta}^*$ is a $(N \times 1)^2 \times (N + 1)^2$ matrix, $\overline{\alpha\beta}^*$ is a $(I \cdot J \cdot 3) \times (N + 1)^2$ matrix, the transpose of $\overline{\alpha\beta}$. It should be noted that the monopole ($n = 0$) component occurring in Equation (10) represents the effect of the warped current sheet on the magnetic field. The original polarity of such calculated field lines is finally restored thus ensuring that $\nabla \cdot \mathbf{B} = 0$. This introduces current sheets between regions of opposite-polarity field beyond R_{cp}, but the requirement that the total stresses balance across them is satisfied.

3. Calculation

As shown in Section 2, after specification of the free parameters a and R_{cp}, the observed photospheric magnetic field is the only input to the HCCS model required to calculate the magnetic field beyond the photosphere.

We truncate the spherical harmonic expansions of the observed magnetic field on the solar surface above multipole 9 in computing the expansion coefficients, $g_{nm}^\odot$ and $h_{nm}^\odot$ (e.g., Hoeksema, Wilcox, and Scherrer, 1982). These coefficients are uniquely determined by the normal photospheric field distribution and are independent of the free parameter a (Bogdan and Low, 1986; Zhao and Hoeksema, 1993a). The maximum principal index used in calculation above the cusp surface, N_c, is not the same as below the cusp surface, $N_\odot$, due to the reorientation of the magnetic field on the cusp surface. The trial calculation for a dipole field ($N_\odot = 1$) on the solar surface with $a = 0$ and $R_c = 1.6$ used in Schatten's modeling showed that with $N_c = 5$ the model prediction of the magnetic configuration agreed with the full MHD solution. Figure 2 displays the calculated field lines in the case of $N_\odot = 1$ and $N_c = 1, 3, 4, 5$. In the following calculation using the observed photospheric magnetic field for Carrington rotation 1647 as the inner boundary condition, we select $N_\odot = 9$ and $N_c = 13$. Increasing either index had little effect on the result.

The a parameter characterizes the spatial distribution of horizontal electric currents above the solar surface. When $a > 0$ the appropriate magnetic force acts to expand magnetic field lines above the photosphere. The selection of a is a rather difficult task. Because the closed field regions calculated by the PFSS model match the full MHD solution as well as various observations quite well, as mentioned in Section 1, we select such an a value that makes the calculated closed regions below the cusp surface have approximately the same configuration predicted by the source-surface model. Figure 3 displays the calculated magnetic field configuration
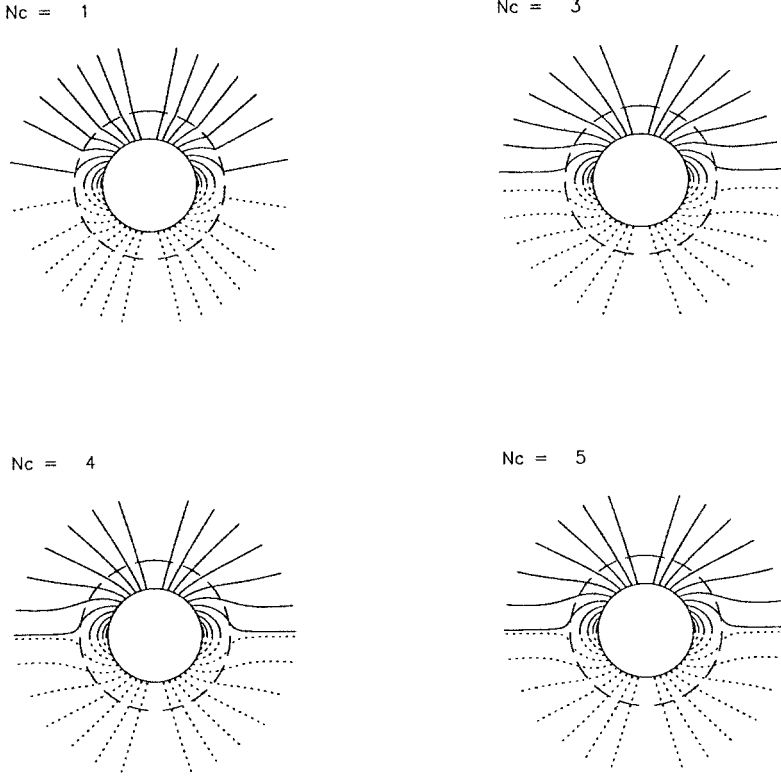
Nc = 1

Nc = 3

Nc = 4

Nc = 5

Fig. 2. The open and closed magnetic field lines calculated using the horizontal current–current-sheet model with the cusp surface at $r = 1.6\,R_\odot$ and free parameter $a = 0.0$. The maximum principal index below the cusp surface is $N_\odot = 1$ (a dipole field). The maximum principal index used above the cusp surface varies from 1 to 5 as indicated for the various panels.

by the HCCS model (solid lines) and the PFSS model (dotted lines) for a dipole field boundary condition. The figure shows that the optimum choice appears to be $a = 0.25$ for which the field lines predicted by the HCCS model (solid lines) are almost completely aligned with those predicted by the PFSS model below about $2.0\,R_\odot$.

It may be appropriate to mention that unless a steady electric current is explicitly required to be continuous across a boundary, in general only the normal component of the steady electric current will be continuous due to $\nabla \cdot (\nabla \times \mathbf{B}) \equiv 0$. In a force-free magnetic field model there must be a radial component to form field-aligned currents, therefore the boundary conditions of the system must provide information about the electric current. Unlike the force-free field model, there are only transverse electric current components in the HCCS model. Unless the boundary is required to be continuous for the transverse components as well as the normal component, it is reasonable to use the observed line-of-sight field observations as a boundary condition of the model, even though this provides no
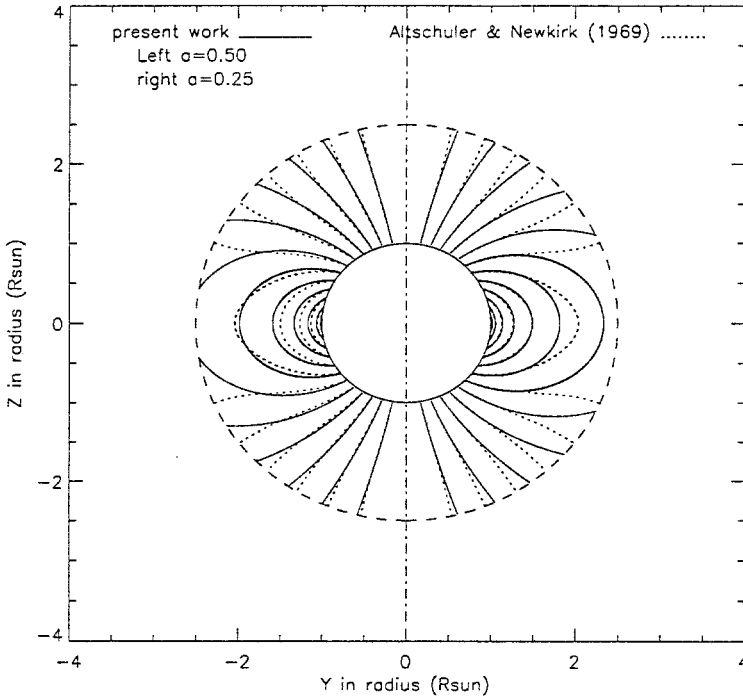
Fig. 3. Comparison of the magnetic field configuration calculated from the horizontal current–current-sheet model (solid lines) using the free parameter $a = 0.25\,R_\odot$ (*right*) and $a = 0.5\,R_\odot$ (*left*) with that from the source-surface model (dotted lines) using the source surface at $r = 2.5\,R_\odot$. The boundary condition used in calculation is a dipole field. The comparison can be used to select an optimum value of a.

information about the electric current on the inner boundary. In fact, boundaries used in global mapping are usually discontinuities for the transverse components of steady electric currents. For example, the solar surface and the source surface boundaries are discontinuities for transverse components of both magnetic field and electric current in the PFSS model (Wang and Sheeley, 1992; Zhao and Hoeksema, 1993).

As defined in Section 2, the heliocentric distance of the cusp surface, R_{cp}, is determined by the altitude of the cusp-type neutral points of helmet streamers in solar eclipse images. In practice, observed cusp points occur at different heights. Their average value is probably a good estimate for R_{cp}. The preliminary choice of the optimum R_{cp} may be inferred by matching the trial calculations for a dipole field to the Pneuman and Kopp solution. In the following calculation we take $R_{cp} = 2.25$.

Figure 4(a) displays the magnetic configuration predicted by the PFSS model, the PFCS model and the expanding isothermal MHD model, showing the agreement of the calculated closed regions between the PFSS and MHD models, and the agreement of the calculated open field regions between the PFCS and the MHD
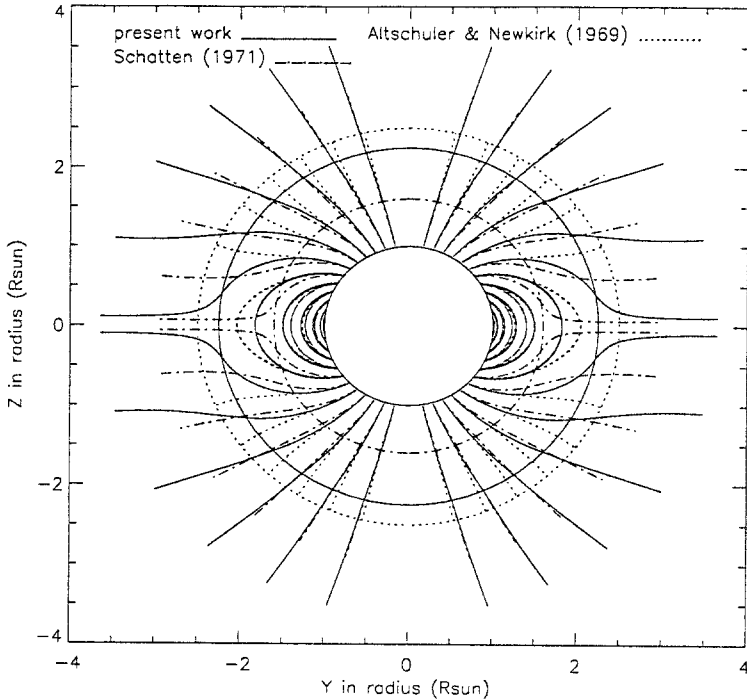
Fig. 4.   Comparison of the magnetic field configurations calculated using various models. (a) The magnetic configuration predicted by the PFSS, PFCS, and expanding isothermal MHD models (from Schatten, 1971). (b) The magnetic field lines calculated from three models by using a dipole photospheric field boundary condition. Solid lines are from the HCCS model with $a = 0.25$ and $R_{cp} = 2.25$, dot-dashed lines from the PFCS model with $R_{cp} = 1.6$, and dotted lines from the PFSS model with the source surface at $r = 2.5$.

models. Figure 4(b) displays the magnetic configuration produced by the HCCS model (solid lines), the PFSS model (dotted lines), and the PFCS model (dash-dotted lines). The closed and open field lines predicted by the HCCS model agree very well with the closed field lines predicted by the PFSS model and the open field lines predicted by the PFCS model. Thus the prediction of the present model with $a = 0.25$, $R_c = 2.25$ agrees with the MHD model better than the previous models.

4. Prediction and Comparison

Near solar minimum the white-light corona shows a dipole-like structure, thus the HCCS model is quite likely to be valid in this interval in mapping the observed photospheric field into the corona. Using the WSO synoptic chart of Carrington Rotation 1647 as the boundary condition on the solar surface, the magnetic field lines below the cusp surface are calculated by the HCCS model with $a = 0.25$ (solid lines) and by the PFSS model with the source surface at $2.5\,R_\odot$. Figure 5
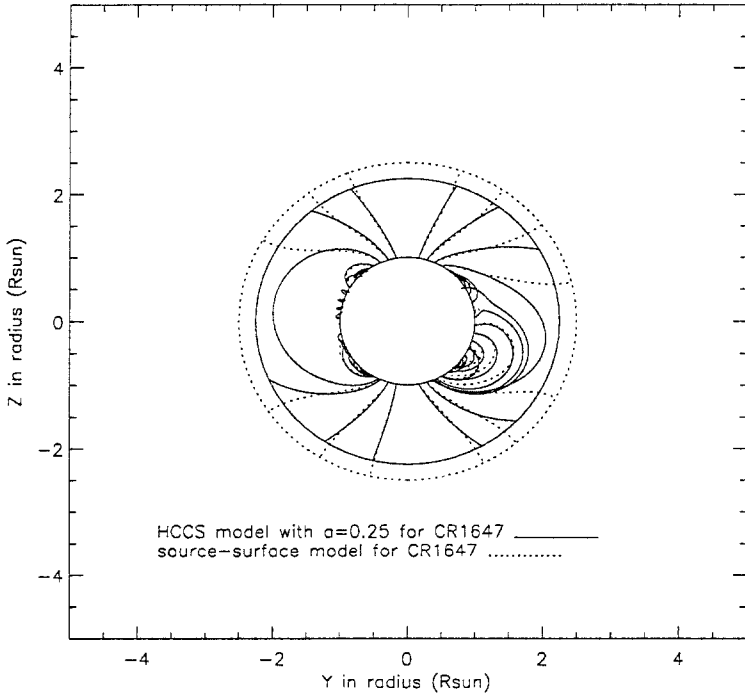
Fig. 5. The same as Figure 3 except using the observed synoptic chart for Carrington rotation 1647 as input to the HCCS model and the source-surface model. The disk center is at Carrington longitude 195°, corresponding to the situation on 23 October, 1976 when a total solar eclipse was observed.

displays the calculated mangetic field configuration on the east and west limbs with 195° at disc center, corresponding to the central meridian passage date of 23 October, 1976, when a total eclipse was observed. The figure shows that the field lines produced by the two models agree well in the lower corona, supporting the inferred value of a in Section 3.

Figure 6 with the same format as Figure 5 displays the calculated magnetic configuration between 1 and 4 solar radii by the HCCS model with $a = 0.25$ and $R_{cp} = 2.25$. To take into account of the possible contributions of features adjacent to the limbs in the eclipse image, we calculate the field lines rooted within a longitudinal interval of 60° centered at 105° (east limb) and 285° (west limb). Comparison of Figure 6 with the eclipse observation (see Figure 1) shows that the helmet structures, the polar plumes, and the axes of coronal streamers are successfully predicted by the present model.

5. Conclusion and Discussion

To compute long-lived, large-scale coronal structures, such as helmet streamers and coronal holes as observed in the white light, EUV, and soft X-ray corona, it has long
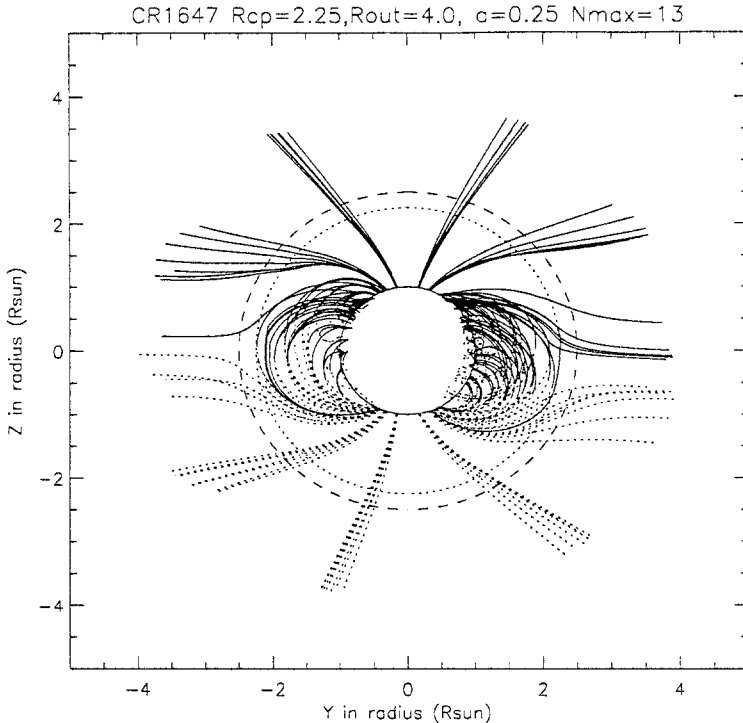
Fig. 6. The magnetic field lines predicted form the HCCS model with $a = 0.25$, $R_{cp} = 2.25$, $N_{\odot} = 9$, and $N_c = 13$. The solid and dotted lines denote lines pointed, respectively, outward and inward. The disk center has a Carrington longitude of $195°$, corresponding to 23 October, 1976 when a total solar eclipse was observed (compare with the top panel of Figure 1).

been desired to develop a model realistic enough to accept observational magnetic and plasma data as primary inputs and to include the interaction between the solar wind and coronal magnetic field. The previously developed PFSS, PFCS, and HCSS models accept observed photospheric magnetic fields as input and partially estimate the solar wind–magnetic field interaction. As pointed out in Section 2, the PFSS model describes the interaction using horizontal volume currents above the source surface and is most successful in reproducing structures in lower corona, especially closed regions and their associated structures. The PFCS model estimates the effect of sheet currents within streamer interfaces and is most successful in predicting open field structures such as polar plumes and the axes of coronal streamers. The HCSS model estimates the effects of the horizontal volume currents below the source surface and allows us to calculate plasma properties between the solar and source surfaces. However, the solar wind–magnetic field interaction results in both horizontal volume currents and sheet currents.

The HCCS model developed here includes both horizontal volume and streamer sheet currents; it can predict closed field regions better than the PFCS model and open field regions better than the PFSS model. Because the open field configuration

calculated using the HCCS model is more accurate than the PFSS model prediction of the observed polar plumes and streamer axes, we intend to investigate whether the HCCS model predicts the magnetic field strength and the flux tube expansion better than the source-surface model.

By introducing volume currents into the inner corona, both the HCSS model and the HCCS model can calculate plasma properties, as shown by Equations (3) and (4). This opens a way to enhance the scientific return from magnetograph observations and other coronal observations, particularly from the upcoming SOHO mission. For example, by using the HCSS model and matching the calculated $r - \theta$ distribution of the electron density at low and middle latitudes to a white-light coronal helmet structure observed on 26 May, 1986 Bagner and Gibson (1991) obtained an axisymmetric magnetic field. By using the observed WSO photospheric magnetic field synoptic chart for Carrington rotation 1780, the observed white-light coronal streamer belt at 1.3 $R_\odot$ for the same solar rotation has also been predicted by the HCSS model (Zhao and Hoeksema, 1992). However, the agreement between predictions and observations is only to the two-dimensional problems. It might not be reasonable to expect that the HCSS model be able to extrapolate the observed photospheric field into the corona and make a prediction of the three-dimensional distribution of the electron density that is consistent with the K-corona observations. The reason is that the plasma properties are much more sensitive to the distribution of electric currents due to the low β coronal plasma than the magnetic field, and the single parameter a in the model is unable to represent both volume and sheet currents flowing in the corona (especially the local sheet currents flowing within the helmet interfaces). The HCCS model developed in this paper is expected to be able to extend the prediction of the plasma properties and magnetic field to larger distances than the HCSS model, but the former has the same limitation for prediction of plasma properties in the inner corona as the later does because the former does not include the effects of sheet currents flowing within streamer interfaces and helmet interfaces on the magnetic field and plasma below the cusp surface. The sheet currents within helmet interfaces would act to adjust the magnetic fields on each of the interface to balance the total stress between the bright coronal helmet and the dark coronal hole. To minimize the effect of sheet currents within helmet interfaces, we have calculate the plasma density and the magnetic field in a polar coronal hole, and the result shows (Zhao and Hoeksema, 1993b) the necessity to account for the effect of streamer sheet currents on the plasma and magnetic field below the cusp surface. The study is being continued.

The free parameter a characterizes the horizontal volume current flowing above the photosphere. The selection of a is essential to the model. One way to select a is by matching the closed field configuration computed using HCCS model with that using the potential–source-surface model. The inferred value of a is 0.25 for the solar minimum phase. The success of the HCCS model in modeling the coronal magnetic field in the solar minimum phase, as shown in Figure 6, supports the validity of the horizontal current assumption used in the model. But is the

assumption valid in other sunspot phases? If so, what are the proper values of a and R_{cp} in the other sunspot phases? We hope to answer these questions in subsequent papers.

Acknowledgements

References

Altschuler, M. D. and Newkirk, G.: 1969, *Solar Phys.* **9**, 131.

Bagenal, F. and Gibson, S.: 1991, *J. Geophys. Res.* **96**, 17663.

Bogdan, T. J. and Low, B. C.: 1986, *Astrophys. J.* **306**, 271.

Hoeksema, J. T., Wilcox, J. M., and Scherrer, P. H.: 1982, *J. Geophys. Res.* **87**, 10331.

Levine, R. H., Altschuler, M. D., Harvey, J. W., and Jackson, B. V.: 1977, *Astrophys. J.* **215**, 636.

Loucif, M. L. and Craag, A.: 1988, in R. C. Altrock (ed.), *Solar and Stellar Coronal Structure and Dynamics*, Sunspot, New Mexico, p. 406.

Low, B. C.: 1985, *Astrophys. J.* **293**, 31.

Newkirk, G.: 1972, in C. P. Sonett, P. J. Coleman, Jr., and J. M. Wilcox (eds.), *The Solar Wind Two*, Scientific and Technical Information Office, NASA, Washington D.C., p. 11.

Pneuman, G. W. and Kopp, R. A.: 1971, *Solar Phys.* **18**, 258.

Schatten, K. H.: 1971, *Cosmic Electrodynamics* **2**, 232.

Schatten, K. H., Wilcox, J. W., and Ness, N. F.: 1969, *Solar Phys.* **9**, 442.

Steinolfsen, R. S., Suess, S. T., and Wu, S. T.: 1982, *Astrophys. J.* **255**, 730.

Wang, Y. M. and Sheeley, N. R., Jr.: 1990, *Astrophys. J.* **355**, 726.

Wang, Y. M. and Sheeley, N. R., Jr.: 1992, *Astrophys. J.* **392**, 310.

Wolfson, R.: 1985, *Astrophys. J.* **288**, 769.

Zhao, X. P. and Hoeksema, J. T.: 1992, in *Coronal Streamers, Coronal Loops, and Solar Wind Composition*, ESA Publications Division, p. 117.

Zhao, X. P. and Hoeksema, J. T.: 1993a, *Solar Phys.* **143**, 41.

Zhao, X. P. and Hoeksema, J. T.: 1993b, in *The Proceedings of the Second SOHO Workshop*, in press.